

# Fast-Framing Optical Imaging of Plasma Formation in Resonant Microwave Pulse Compressor

Leonid Beilin, Anatoli S. Shlapakovski, Moshe Donskoy, Yoav Hadas, Uri Dai, and Yakov E. Krasik

**Abstract**—Plasma evolution in the interference switch of an S-band pulse compressor operating in the frequency of 2.766 GHz, with input pulses of 200–450-kW power and duration of 2.4  $\mu$ s, was studied experimentally and in numerical simulations. The system was filled with dry air at  $2 \times 10^5$ – $3 \times 10^5$ -Pa pressure. The plasma discharge that switches the phases of the compressor operation from energy storage to release was initiated by a Surelite laser. The evolution of the light emission from the plasma was studied using fast-framing optical imaging with a 4QuikE camera. From the obtained typical size of the plasma and its velocity of expansion along the electric field, the density of the plasma was estimated, and the influence of its evolution on the power and waveform of microwave output pulses observed in the experiments was determined in simulations.

**Index Terms**—Microwave pulse compression, plasma switch.

## I. INTRODUCTION

THE method of resonant pulse compression is a promising approach to high-power microwave generation [1], [2]. Resonant compressors employ conventional pulsed magnetrons or klystrons as primary sources to generate nanosecond (ns) microwave pulses of  $10^6$ – $10^9$ -W peak power. In this type of compressor, the RF energy is stored in a high- $Q$  cavity providing a high power gain, and the extraction of the stored energy is achieved using a fast interference switch. The switch is a key element, because it should open the cavity in the ns time scale to release the energy into a load. An ideal switch would open the cavity fully and instantly, providing an output pulse having a rectangular waveform, a duration equal to the double transit time of an electromagnetic (e/m) wave along the cavity, and power corresponding to that of a traveling wave in the cavity before switching. However, in existing high-gain compressors with plasma switching, the waveform of output pulses is far from being rectangular, and the power is significantly lower. For instance, in the S-band compressor with a gain of 23 dB [3], the output power was lower by a

factor of 1.5. For the X-band compressor with a 20-dB gain, an output power reduction by a factor of two was reported [4].

Despite various experimental studies of compressors based on plasma interference switches, at present, there is no clear understanding of the processes that govern the plasma formation under a strong RF electric field in pressurized gases and ultimately determine a compressor's output power. Evidently, the output waveform distortion and power losses are determined by neutrals ionization and excitation, electron scattering dynamics, and microwave energy dissipation in the plasma at the initial stage of its formation and evolution. In high-power compressors operating at high pressures of the background gas, the plasma is characterized by a high rate of electron-neutral collisions. The electron avalanche should occur in the sub-ns timescale to form plasma with conductivity sufficient to break the destructive interference of e/m waves in the switch, while keeping to a minimum the losses of microwave energy due to Joule heating of the plasma. There are many theoretical, numerical, and experimental research studies related to microwave gas breakdown [5]. However, the process of the plasma formation was not considered in connection with the microwave energy storage in and release from the resonant compressor. For instance, there are no data concerning the size and density of the plasma needed for relatively efficient energy extraction.

The main purpose of this paper is to study the plasma evolution in a resonant microwave pulse compressor with an H-plane waveguide tee as an interference switch using a fast-framing 4QuikE intensified camera (optical imaging was applied earlier to characterization of the ns discharge in the gas-filled diode [6]). The results of observations of the light emission from the plasma are used to obtain the typical size of the plasma, the velocity of its expansion along the electric field, and its density.

## II. EXPERIMENTAL SETUP AND RESULTS

Experiments were performed using the configuration of the compressor shown in Fig. 1, assembled of WR284-waveguide-based parts (72-mm  $\times$  34-mm cross section). The compressor was charged by a frequency-tunable CPI VMS1177 magnetron, generating pulses of 200–450-kW power and up to 2.4- $\mu$ s duration. For the compressor cavity, the 40-dB directional coupler was employed, so that the power of the traveling wave component of the cavity field could be measured directly. The input signal entered the cavity through the iris having a coupling hole 27 mm in diameter; the opposite end was connected to the H-plane tee with the side arm shorted by a copper

Manuscript received February 9, 2014; accepted March 30, 2014. Date of publication April 18, 2014; date of current version May 6, 2014. This work was supported in part by Technion under Grant 20003813 and in part by the Binational Science Foundation under Grant 1009212.

L. Beilin, A. S. Shlapakovski, M. Donskoy, and Y. E. Krasik are with the Plasma and Pulsed Power Laboratory, Department of Physics, Technion, Haifa 32000, Israel (e-mail: leonidus@tx.technion.ac.il; shl@physics.technion.ac.il; moshe.dnsk@gmail.com; fnkrasik@physics.technion.ac.il).

Y. Hadas is with the Department of Applied Physics, Rafael, Haifa 31021, Israel (e-mail: yoavhadas@yahoo.com).

U. Dai is with DDR&D/IMOD, Tel Aviv 61909, Israel (e-mail: uri\_dai@mod.gov.il).

Color versions of one or more of the figures in this paper are available online at <http://ieeexplore.ieee.org>.

Digital Object Identifier 10.1109/TPS.2014.2316204

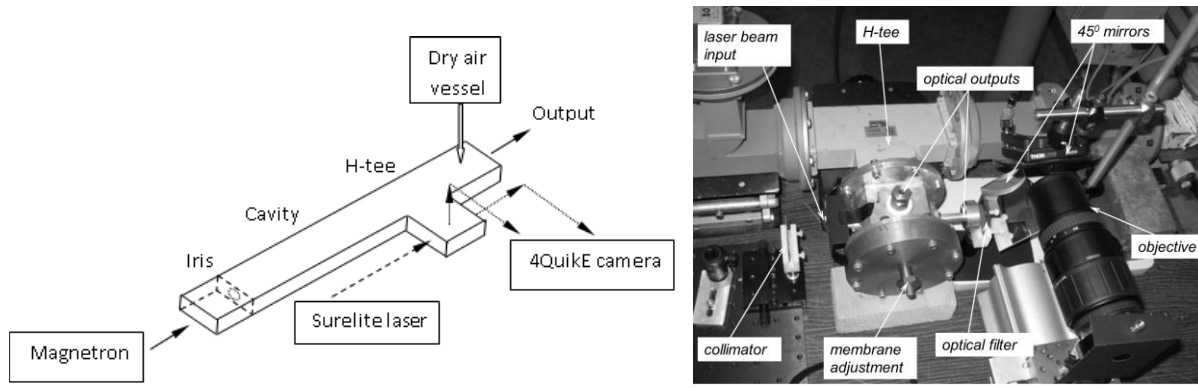


Fig. 1. Left: schematic of the experimental setup. Right: setup for fast-framing imaging of the microwave plasma discharge.

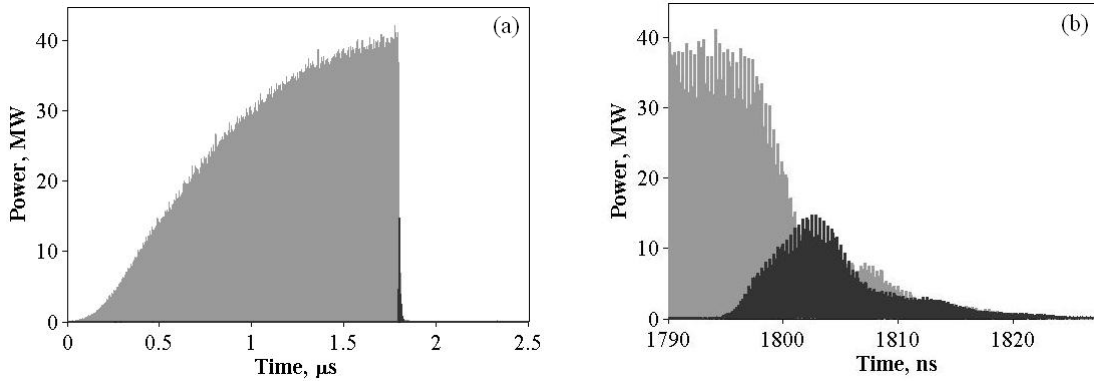


Fig. 2. (a) Instantaneous power of the output (dark gray) and cavity signals recorded when the maximal output power was achieved. (b) Same as (a) in the ns timescale.

membrane. The membrane deformation was adjusted such that the compressor resonant frequency coincided with the closing frequency of the tee. When this was the case, the resonant frequency  $f = 2.766$  GHz was measured with an R&S ZVL network analyzer at  $P \sim 2 \times 10^5$ -Pa pressure of dry air inside the system.

For the energy release, the Surelite laser beam ( $\lambda = 532$ -nm,  $\sim 50$ -mJ,  $\sim 7$ -ns FWHM) collimated by a 1-mm diameter hole at the entrance into the tee side arm was used to initiate the plasma discharge at a quarter guide wavelength ( $\sim 40$  mm) from the membrane. The light emitted from the plasma was observed both in side-view imaging, when the light was collected through the 5-mm diameter hole in the narrow wall of the tee waveguide, and in top-view imaging, when the light was collected through the slot (7 mm  $\times$  2 mm) made along the centerline of the wide wall of the waveguide. In the case of the side-view imaging shown in Fig. 1, an optical filter blocking the laser light was placed after the optical output. Using two 45° mirrors and lenses, the light from the plasma was focused onto the photocathode of a 4QuikE camera operating with a 2-ns frame duration. For the calibration of the image dimensions, an optical target with a graduated pattern was placed in the middle of the waveguide; a resolution of  $\sim 7.35$   $\mu\text{m}/\text{pixel}$  was obtained.

Experiments were conducted at different gas pressures and input power of the magnetron. The magnetron power that

the compressor cavity withstands during the charging stage without a self-breakdown increased with increasing pressure; the output power of the compressor increased accordingly. The maximum output power of  $\sim 7.4$  MW was obtained at  $P = 3 \times 10^5$  Pa when the input power was  $\sim 420$  kW and the peak power of the cavity field traveling wave component was  $\sim 21$  MW. The instantaneous powers calculated from the oscilloscope traces of RF voltages obtained in this case for the cavity and output signals are shown in Fig. 2. One can see that the FWHM of the output pulse is  $\sim 8$  ns, the rise time (0.1–0.9 of maximum) is  $\sim 5$  ns, and the maximal efficiency of power extraction is  $\sim 35\%$ . At lower pressures, power extraction was found to be less efficient. The waveform of the output pulse is typical for any pressure.

Several side-view photo-sessions were performed at different pressures with different camera gains. For each framing image of the plasma light emission, the corresponding camera synchro-pulse and the compressor microwave output pulse were recorded. The time shift  $\Delta_{c-\mu w}$  of the beginning of the 2-ns frame with respect to the start of the microwave extraction (the moment of time at which the RF voltage in the output pulse reaches 10% of its maximum) was determined for each recorded image. Typical side-view images showing the dynamics of the plasma formation at the pressure  $P = 2 \times 10^5$  Pa are shown in Fig. 3. One can see that at  $\Delta_{c-\mu w} = -5.1$  ns, i.e., before the beginning of the microwave

TABLE I

$\Delta_{c-\mu w}$ (ns)	Length (mm) (bright part only)	Width (mm) (bright part only)	Width (mm) (bright part + diffusive part)
-5.1	0.5	0.1	Not seen
-2	0.7	0.1	Not seen
-1	1	0.1	0.5
0.5	1.3	0.2	0.7
1.9	2.3	0.3	0.8
8.5	5.7	0.4	0.8

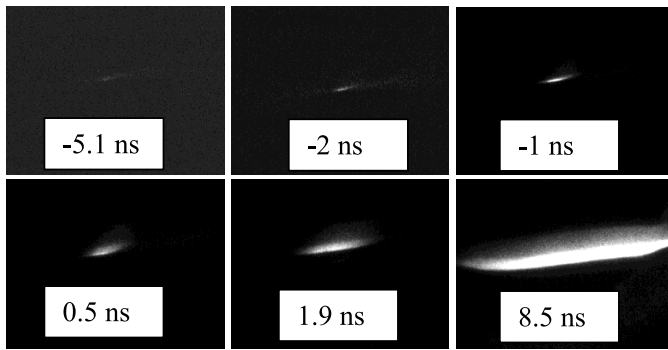


Fig. 3. Side-view images recorded at  $2 \times 10^5$ -Pa pressure with 4QuikE camera at different time shifts  $\Delta_{c-\mu w}$ . The exposure time is 2 ns; the camera gain is close to maximal one. The input power is of  $\sim 310$  kW.

extraction, the recorded region of light emission from the plasma has small dimensions of  $\sim 0.5$  mm in length and  $\sim 0.1$  mm in width. With an increase in the value of  $\Delta_{c-\mu w}$ , one obtains an increase in the dimensions of the plasma, mainly along the direction of the RF electric field, and at  $\Delta_{c-\mu w} = 8.5$  ns, which corresponds to the maximum of the output power, the light emitting plasma occupies almost the whole diameter of the output window. Let us note here that the light emission region is actually parallel to the electric field, and visible deflection of the images from the horizontal line is related to the optical setup. One can see also a rather sharp light emission boundary from the cavity waveguide side and a diffuse light emission boundary from the copper membrane side. This agrees with the qualitative explanation that denser and high-temperature plasma should be formed at the side of the input of the e/m wave.

The estimated dimensions of the light emission regions shown in Fig. 3 are summarized in Table I. These data can be used for an analysis of the plasma evolution in the ns timescale during the extraction of the compressor output pulse. It is understood that an analysis of this kind is justified only for a small enough time jitter of the microwave output pulse with respect to the triggering laser pulse. In the case of the images shown in Fig. 3, the jitter in the corresponding series of pulses was determined to be  $\sim 2.7$  ns, which can be considered acceptable. In addition, for this case ( $\sim 310$ -kW input power),

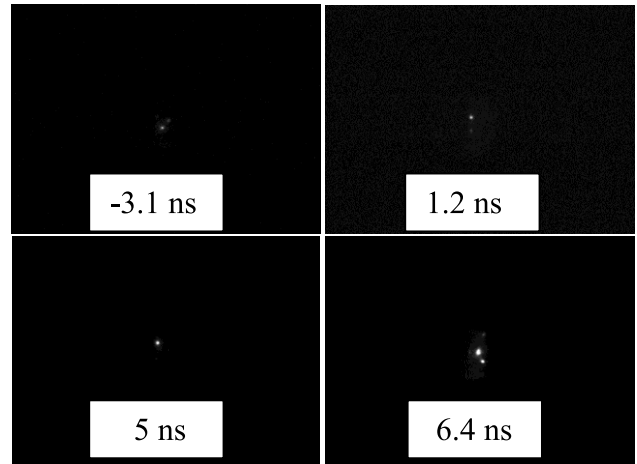


Fig. 4. Top-view images recorded at  $2 \times 10^5$ -Pa pressure with 4QuikE camera with 3-ns exposure time at different time shifts  $\Delta_{c-\mu w}$ .

the average time delay between the laser beam entering into the system and the start of the microwave extraction was  $\sim 24$  ns. It was found that with decreasing input power, this time delay increases, and the jitter increases as well. An increase in the input power resulted in an unacceptably frequent appearance of the microwave output prior to the laser pulse.

Light emission images obtained at a higher pressure,  $P = 3 \times 10^5$  Pa, and, respectively, at a higher input power,  $\sim 420$  kW, are very similar to those shown in Fig. 3. In this case, the time delay between the laser beam appearance in the tee side arm and the beginning of the microwave extraction increased up to  $\sim 43$  ns; the time jitter, however, increased insignificantly, up to  $\sim 3.8$  ns.

Similarly to side-view imaging, several top-view photo-sessions at different pressures were conducted. Typical top-view images recorded at  $2 \times 10^5$ -Pa pressure at different  $\Delta_{c-\mu w}$  are shown in Fig. 4. From the images in Figs. 3 and 4, one can conclude that the discharge channel represents a filament-like structure. Let us note here that in most of the framing images, there was only one filament (seen as a point), but in a small number of discharges also two, three, and even four filaments were obtained. The diameter of the filaments was in the range of 0.2–0.6 mm.

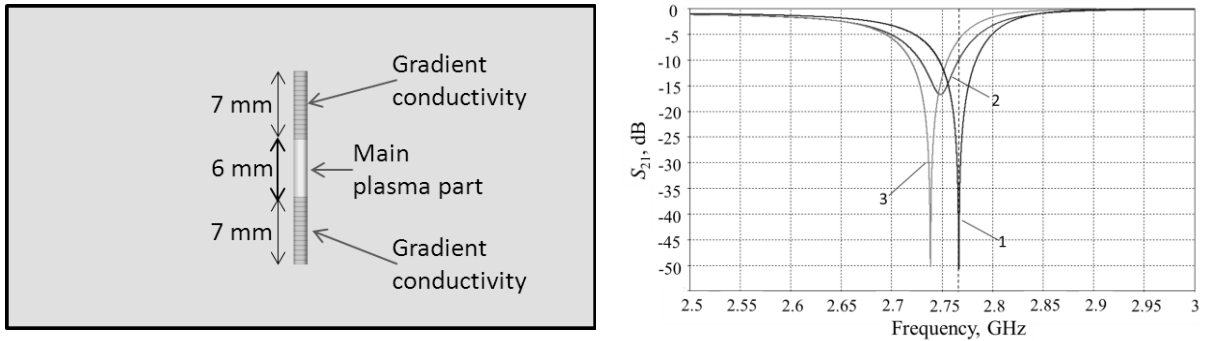


Fig. 5. Left: configuration of the conductive gas (plasma) filament in the WR284 waveguide cross section taken for CST simulations. Right: frequency response of the H-plane tee with the conductive gas filament in the shorted side arm. The conductivity in the main part  $\sigma_0 = 1-0$ ;  $2-2.3 \times 10^3 \Omega^{-1}\text{m}^{-1}$ ;  $3-2.7 \times 10^7 \Omega^{-1}\text{m}^{-1}$ . The vertical dashed line shows the closing frequency of the tee in the absence of plasma.

### III. DISCUSSION AND NUMERICAL MODELING

From the results of optical imaging of the plasma formation in air, one can estimate roughly the main plasma parameters. Using the data shown in Table I, the average drift velocity of the discharge channel propagation along the electric field can be evaluated as  $V_d \sim 5 \cdot 10^5$  m/s. This allows one to estimate the effective electron-neutral collision frequency  $\nu = eE/mV_d$  [5], where  $E$  is the electric field in the discharge location, and  $e$  and  $m$  are the electron charge and mass, respectively. For  $E \sim 7 \times 10^6$  V/m (this corresponds to the cavity signal measured), one obtains  $\nu \approx 2.5 \times 10^{12}$  s $^{-1}$ . Now, assuming that the width of the bright part of the plasma image represents the effective thickness of the skin layer  $\delta$  and using formulas connecting the conductivity  $\sigma$  of a strongly collisional plasma ( $\nu \gg 2\pi f$ ) with the skin layer thickness, on the one hand, and the electron density  $n_e$ , on the other hand

$$\sigma = \frac{c^2}{4\pi^2 f \delta^2} = \frac{e^2 n_e}{m \nu}$$

one can estimate the plasma density as  $n_e \approx 2 \times 10^{17}$  cm $^{-3}$  for  $\delta = 2 \times 10^{-2}$  cm. It is understood that this estimate does not account for the time evolution of the electric field around a conductive plasma filament; it gives only an upper limit for the electron density, since a visible image cannot be wider than the skin layer.

Having the estimates of the plasma parameters, one can find the characteristics of the compressor output signal using numerical simulations and compare them with those obtained in the experiments. The extraction efficiency, i.e., output-to-cavity power ratio, can be determined by calculating the transmission coefficient  $S_{21}$  between two collinear arms of the H-plane waveguide tee with the shorted side arm containing plasma inside. To do this, CST simulations [7] were carried out. The position of the shorting plane in the side arm was taken to give the same calculated closing frequency of the tee as the compressor operating frequency. The plasma was represented as a 0.6-mm diameter cylindrical column with a given conductivity, oriented along the RF electric field, and located symmetrically with respect to the center of the waveguide cross section in the antinode of the field

closest to the shorting plane. Initial simulations with the 6-mm long uniform plasma column (as the bright part of the images observed when the exposure time corresponded to the peak in the output power) did not result in a substantial transmission at the operating frequency, even for a perfect conductor. Then, the conductivity distribution along the column shown in Fig. 5 was considered. Namely, extensions to the main part of the plasma column were introduced to represent significantly less intensive light emission, i.e., the conductivity was taken to be constant,  $\sigma = \sigma_0$  in the 6-mm long central part of the filament and exponentially decreasing,  $\sigma = \sigma_0 \exp\{-[(|z| - 3[\text{mm}])/1[\text{mm}]]\}$  ( $z$  is the coordinate) in the 7-mm long extensions. With this conductivity profile, the calculated transmission coefficient at the operating frequency rises as high as  $-10$  dB for the value of  $\sigma_0$  corresponding to the above estimate of the plasma density  $n_e \approx 2 \times 10^{17}$  cm $^{-3}$  (curve 2 in Fig. 5). This is roughly in agreement with the extraction efficiency obtained at  $2 \times 10^5$ -Pa pressure.

A more detailed comparison with experimental results is possible through simulations using the MAGIC code [8], allowing one to observe the dynamics of the process of microwave extraction from the compressor cavity. The plasma was simulated by the gas conductivity model embedded in the MAGIC code, which accounts for electron avalanche, attachment to neutrals, and recombination with positive ions. The plasma conductivity in this model is determined by the electron and ion densities and mobilities depending on the electric field, pressure, and temperature. The simulations started from the preset RF fields obtained in the simulations of the compressor charging; the electric field pattern (together with the simulation geometry) and build-up in time are shown in Fig. 6. The initial electron density was set to be zero, and at a certain time from the start of the simulation, the external ionization rate (source term) was turned on. For setting the source term, the results of light emission imaging presented in Section II were taken into account.

It was assumed that the ionization occurs in the rectangular column of the 1-mm  $\times$  1-mm cross section oriented along the  $z$ -coordinate (field direction) in the field antinode closest to the shorting plane in the tee side arm. The ionization

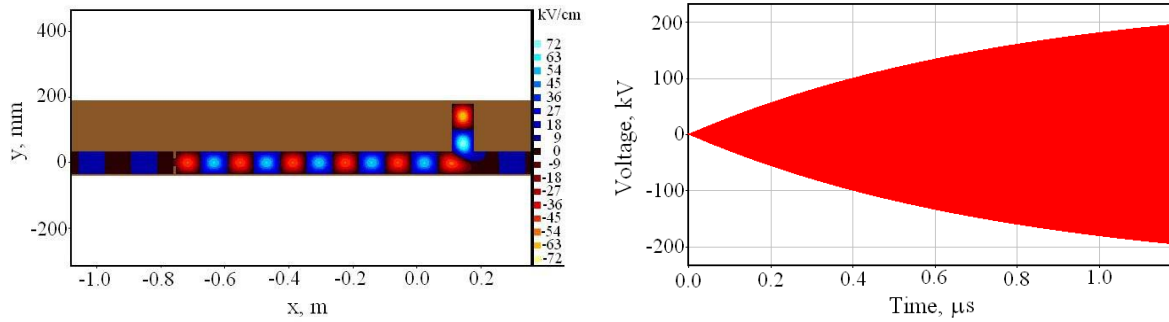


Fig. 6. Results of the MAGIC simulation of the compressor charging used to preset initial fields in simulations of microwave extraction. Left: contour plot of the  $E_z$ -field in the  $x$ - $y$  plane. Right: build-up of the RF voltage across the waveguide in the field antinode in the middle of the cavity (between the input iris and tee side arm). The voltage amplitude of the wave entering the system in the  $TE_{10}$  mode is 15 kV.

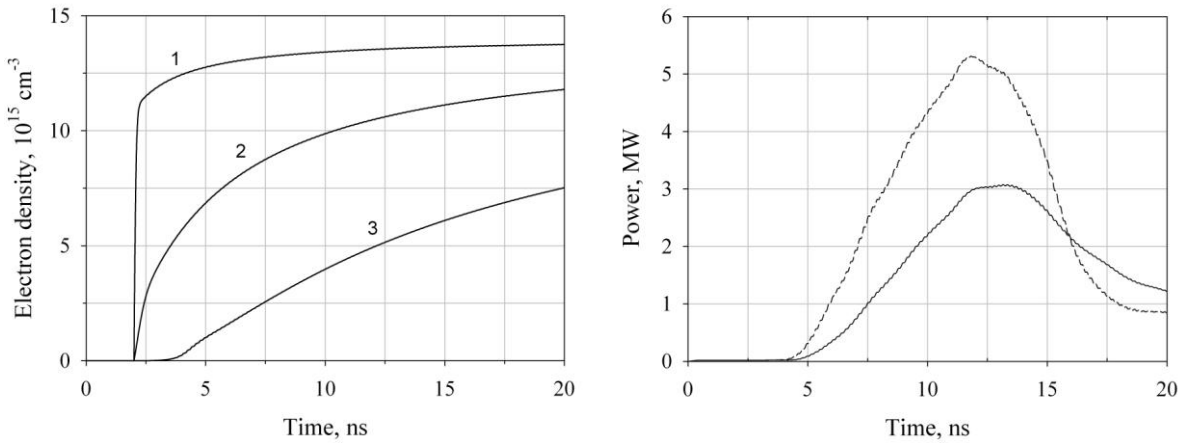


Fig. 7. MAGIC simulation of the energy release from the compressor cavity in the gas conductivity model for air at  $2 \times 10^5$ -Pa pressure for  $Q_0 = 2 \times 10^{26} \text{ cm}^{-3} \cdot \text{s}^{-1}$ . Left: electron density within the plasma filament versus time at  $z =$ : 1–0.5 mm; 2–3.5 mm; 3–12.5 mm. Right: microwave power at the output port versus time (dashed curve is for the case  $Q_0 = 10^{27} \text{ cm}^{-3} \cdot \text{s}^{-1}$ ).

rate  $Q$  was set depending on  $z$  and time:  $Q = Q_0 \Theta(t - t_0) \exp\{-|z|/[z_0 + V(t - t_0)]\}$ . This function describes the plasma filament, which appears at the moment  $t_0$ , whose density is maximal at the waveguide center and evanesces in the directions toward the walls. The scale of evanescence linearly increases in time from the value  $z_0$  with the rate  $V$ , thus modeling the plasma expansion due to electron diffusion. For the simulations, the values  $z_0 = 1$  mm,  $V = 5 \times 10^5$  m/s, and  $t_0 = 2$  ns were used. The amplitude  $Q_0$  was a variable parameter determining the electron density and, respectively, the conductivity in the filament. The results of the MAGIC simulation with  $Q_0 = 2 \times 10^{26} \text{ cm}^{-3} \cdot \text{s}^{-1}$  illustrating the process of microwave energy extraction from the compressor are shown in Fig. 7. In the left plot of Fig. 7, the time dependences of the electron density at different distances from the middle of the filament ( $z = 0$ ) are presented. For the point close to the middle ( $z = 0.5$  mm, curve 1), one can see a steep rise after turning on the source term and a following slight increase. It is the source term that determines the fast initial growth of the density, which is terminated when the external ionization is compensated by the recombination process. The further slight increase is caused by the expansion of the plasma filament, as a result of which the density in

the observation point approaches the density in the middle. Obviously, at greater distances from the middle, the initial rise is slower, and the following increase is steeper. The process of the filament expansion actually shapes the waveform of the output pulse shown in the right plot of Fig. 7. Indeed, the plasma appearance breaks the destructive interference of e/m waves in the H-plane tee, as a result of which the microwave energy is accumulated in the cavity and its leakage to the output is negligible. As the volume occupied by the plasma increases, the leakage becomes more and more significant and the output power rises. The output power is also higher for a higher density of the plasma in the same volume, a density produced by a larger source term (dashed curve in Fig. 7).

A comparison of the time dependence of the output power obtained in the simulation (the right plot of Fig. 7) with the typical waveform of the compressor output pulses (Fig. 2) shows good agreement. One can evaluate the rise time from the curves in Fig. 7 as  $\sim 5.4$  ns (0.1–0.9 of maximum). The fact that the compressor output pulse rise time was almost the same as in the simulation with the parameter  $V$  taken from the processing of images confirms the correctness of the processing. In addition, the peak output power of  $\sim 3$  MW in the simulation with  $Q_0 = 2 \times 10^{26} \text{ cm}^{-3} \cdot \text{s}^{-1}$  agrees with

the experimentally measured power at  $2 \times 10^5$ -Pa pressure. It should be noted that the said peak power corresponds to a plasma density of  $\sim 1.4 \times 10^{16} \text{ cm}^{-3}$ , which is an order of magnitude lower than the rough estimate made at the beginning of this section. However, the filament transverse size used in these simulations was actually twice that observed in the experiment. Simulations with an appropriate cross section of the filament, furthermore, expanding in time, would give a higher plasma density corresponding to the same microwave power.

To conclude, the results of the simulations showed that the efficiency of the microwave power extraction from the compressor cavity and the rise time of the output pulse depend on the rate of external ionization and the velocity of the plasma filament expansion. These parameters determine the plasma density and the volume it occupies; the higher the density and the larger the volume, the higher the output power. It is significant that, in the case of a small volume, the plasma, even assuming it to be a perfect conductor, would not result in any considerable microwave extraction. Simulations with the measured velocity of plasma expansion give an output pulse rise time of  $\sim 5.4$  ns and extraction efficiency of up to 35%, as observed in the experiments. Evidently, in experiments where laser triggering is used, a filament sufficiently long for efficient extraction would be formed much faster if the laser beam were directed along the electric field line, i.e., normally to the wide wall of the waveguide. A corresponding investigation is worthwhile.

#### IV. CONCLUSION

Using time- and space-resolved imaging of the light emission, the ns dynamics of the plasma formation in an interference switch of a high-power microwave pulse compressor was experimentally observed. The plasma has the form of filaments expanding along the RF electric field. By applying the data obtained from fast-frame imaging, the parameters of the plasma—density and collision frequency—were estimated. Numerical simulations of the microwave energy release from the compressor cavity after the appearance of such a plasma filament with the expansion velocity taken from the imaging data demonstrate a good agreement of the microwave output pulse waveform with those obtained in the experiments. The rather low ratio of the output power to the power of the traveling wave component of the cavity field is caused by a relatively slow dynamics of the plasma formation. To increase the efficiency of the power extraction from the cavity and shorten the rise time of the output pulse, one needs a faster expansion of the plasma filament and/or higher rate of ionization produced by a laser beam triggering the high-pressure discharge.

#### REFERENCES

- [1] J. Benford, J. A. Swegle, and E. Schamiloglu, *High Power Microwaves*, 2nd ed. New York, NY, USA: Taylor & Francis, 2007.
- [2] A. N. Didenko and Y. G. Yushkov, *Powerful Microwave Pulses of Nanosecond Duration*. Moscow, Russia: Energoatomizdat, 1984.
- [3] S. N. Artemenko, V. A. Avgustinovich, and S. A. Novikov, "Single-mode interference switches of high power resonant microwave compressors," in *Proc. 14th SHCE*, Tomsk, Russia, 2006, pp. 410–412.

- [4] S. N. Artemenko, V. A. Avgustinovich, V. L. Kaminskii, P. Y. Chumerin, and Y. G. Yushkov, "Experimental investigation of a 25-MW microwave (3-cm range) compressor prototype," *Tech. Phys.*, vol. 45, no. 12, pp. 1608–1611, Dec. 2000.
- [5] Y. P. Raizer, *Gas Discharge Physics*. Berlin, Germany: Springer-Verlag, 1991.
- [6] S. Yatom, V. Vekselman, G. Z. Gleizer, and Y. E. Krasik, "Space- and time-resolved characterization of nanosecond time scale discharge at pressurized gas," *J. Appl. Phys.*, vol. 109, no. 7, pp. 073312-1–073312-5, Apr. 2011.
- [7] (2013). *CST-Microwave Studio* [Online]. Available: <http://www.cst.com>
- [8] B. Goplen, L. Ludeking, D. Smithe, and G. Warren, "User configurable MAGIC code for electromagnetic PIC calculations," *Comput. Phys. Commun.*, vol. 87, nos. 1–2, pp. 54–86, May 1995.



**Leonid Beilin** received the B.Sc. and M.Sc. degrees in physics from the Technion–Israel Institute of Technology, Haifa, Israel, in 2006 and 2010, respectively, where he is currently pursuing the Ph.D. degree with the Plasma and Pulsed Power Laboratory, Department of Physics.

He is involved in nanosecond timescale plasma formation in the presence of high-intensity electromagnetic field at Technion.



**Anatoli S. Shlapakovski** received the M.Sc. degree in physics from Kharkov State University, Kharkov, Ukraine, and the Ph.D. degree in particle beam physics from Tomsk Polytechnic University, Tomsk, Russia, in 1979 and 1987, respectively.

He joined the Nuclear Physics Institute, Tomsk Polytechnic University, in 1980, where he was involved in high-current charged particle beam physics and high-power microwaves. Since 2009, he has been with the Plasma and Pulsed Power Laboratory, Physics Department, Technion, Haifa,

Israel.



**Moshe Donskoy** received the B.Sc. degree in physics from the Technion–Israel Institute of Technology, Haifa, Israel, in 2010, where he is currently pursuing the M.Sc. degree with the Plasma and Pulsed Power Laboratory, Department of Physics.

He is involved in plasma formation in high pressure and the presence of high-power electromagnetic waves at Technion.

**Yoav Hadas**, photograph and biography not available at the time of publication.

**Uri Dai**, photograph and biography not available at the time of publication.



**Yakov E. Krasik** received the M.Sc. and Ph.D. degrees in physics from the Tomsk Potechnical Institute, Tomsk, Russia, and the Joint Institute for Nuclear Research, Dubna, Russia, in 1976 and 1980, respectively.

He was with the Nuclear Physics Institute, Tomsk, from 1980 to 1991, and the Weizmann Institute of Science, Rehovot, Israel, from 1991 to 1996. He has been with the Plasma and Pulsed Power Laboratory, Department of Physics, Technion, Haifa, Israel, since 1997, where he is currently a Professor. His current research interests include pulsed current-carrying plasmas.